Journal of Computer Assisted Tomography
16(1):41–47, January/February

Signal-to-Noise and Contrast in Fast Spin Echo (FSE) and Inversion Recovery FSE Imaging

R. Todd Constable, Robert C. Smith, and John C. Gore

Abstract: Fast spin echo (FSE) imaging has recently experienced a renewed enthusiasm in the clinical setting for its ability to provide high contrast T2-weighted images in short imaging times. This article evaluates the signal-to-noise ratio (SNR) and contrast-to-noise ratio (CNR) properties of the FSE sequence, inversion recovery (IR) FSE sequence, and conventional SE imaging. The results indicate that FSE imaging displays similar contrast properties to SE imaging, but that the SNR and CNR are improved secondary to the longer TRs and longer effective TEs that may be used. The SNR per unit time of the FSE sequence, and hence its efficiency, is at least a factor of 8 better than the SE sequence when 16 echoes are acquired for each excitation. The addition of a slice selective inversion pulse in IR-FSE allows rapid generation of IR images with image contrast similar to that of conventional IR sequences. When used with a multicoil array for abdominal, pelvic, and spine imaging, the IR-FSE sequence produces images that are virtually free of motion artifact from the subcutaneous fat immediately adjacent to the coils. Both FSE and IR-FSE, when compared with SE imaging, provide superior image contrast and SNR in reduced imaging time. **Index Terms:** Magnetic resonance imaging, techniques—Magnetic resonance imaging, fast spin echo (FSE)—Noise.

Fast scan techniques in the recent past have been dominated by gradient echo sequences that can provide images with various types of contrast with reduced physiologic motion artifacts. These sequences, however, suffer from increased susceptibility, chemical shift and field inhomogeneity effects, and poor T2-dependent contrast when compared with SE imaging (1,2). Gradient echo imaging sequences include echo planar imaging (EPI) (3) and a number of small flip angle techniques such as FLASH, GRASS, FISP, etc. (4–6). Echo planar imaging, while representing the fastest of the MR sequences (an entire image may be collected in $\leq$50 ms), is the most difficult to implement as it requires special hardware and places severe constraints on the gradient coils, coil amplifiers, and receiver capabilities. In practice, this sequence produces images with relatively low resolution and signal-to-noise ratio (SNR). Many of the other gradient echo techniques are available on commercial scanners, and these sequences provide mostly T1-weighted or density-weighted contrast in imaging times ranging from milliseconds, in turbo-FLASH, to minutes. Several reviews on the contrast- and signal-to-noise behavior of these sequences have been published (1,2,7,8). All of the above gradient field echo sequences suffer from loss of signal due to field inhomogeneities and hence can be used only for short TE imaging. Spin preparation pulses have been added to the beginning of a number of these gradient echo sequences, which aid in producing some T2 weighting (9,10).

The fast SE (FSE) sequences include RARE imaging (11,12), first developed by Hennig, and HYBRID (13,14). These sequences can provide strongly T2-weighted contrast in short imaging times, but have previously not gained acceptance in the clinical environment partly because imperfect refocusing pulses produced stimulated echo artifacts (15,16) and also because they resulted in high RF power deposition due to the large number of 180 pulses applied in quick succession in RARE. Additional problems were associated with using nonlinear gradients in HYBRID. Recently, variants of the

From the Department of Diagnostic Radiology, Yale University, 333 Cedar St., New Haven, CT 06510, U.S.A. Address correspondence and reprint requests to Dr. R. T. Constable.

RARE imaging method have attracted renewed interest (17–19) and, through the use of improved 180 pulses and gradient nulling to eliminate spurious features, appear to perform well without serious artifacts. In addition, a better understanding of the role of *k*-space trajectories and contrast behavior in variable TE imaging has led to the development of sequences characterized by smooth, but narrow, point spread functions (PSFs) and hence reduced artifacts at any effective TE. In the sequence described below, the operator is free to choose the echo train length (ETL: the number of echoes and hence phase encode steps per 90° RF excitation pulse), the spacing between the echoes in the echo train, the TR, and the effective TE, which is defined as the TE for the echo associated with the zeroth and other low-order phase encode gradients. The sequence is compatible with multislice imaging. In general, every factor of 2 increase in the ETL will lead to a reduction in imaging time by the same factor, provided that the TR is long enough to accommodate all the requisite slices.

This article reports our measurements of the SNR and contrast-to-noise ratio (CNR) properties of the FSE sequence, IR-FSE, and conventional SE imaging. When used in conjunction with a short TI, the IR-FSE sequence can produce images with similar contrast and quality to conventional STIR sequences (20), with an eightfold reduction in scan time. When used with a multicoil phased array, high resolution, strongly T2-weighted, and IR images are readily obtained, as shown below. The suppression of signal from the subcutaneous fat immediately adjacent to the multicoil produces images virtually free of respiratory motion artifacts arising from the abdominal wall.

MATERIALS AND METHODS

All studies were performed on a GE Signa Advantage, 1.5 T scanner. Images of the brain of a normal volunteer were recorded using the three pulse sequences FSE, IR-FSE, and SE. The FSE and SE images were compared over a range of TEs from 40 up to 160 ms. Over this range, both SNRs and CNRs were measured and compared for different tissues. The measurements were made by selecting at least three different regions of interest for each tissue type, including gray matter, white matter, and CSF, and repeating the measurements in two different slices at the level of the lateral ventricles. One volunteer was used for these measurements as we are interested only in interpulse sequence differences in SNR and CNR and not in interpatient differences. The noise measurements were made by measuring the standard deviation of the noise in selected regions adjacent to the brain. Regions of interest were measured adjacent to the brain in both the frequency and the phase encode directions and averaged. The IR-FSE sequence was tested using a fixed TE and TR and a range of TIs from 20 to 400 ms. Unless otherwise noted, five slices, 5 mm thick, with a field of view of 24 cm, were collected in the imaging studies. The ETL for the FSE and IR-FSE sequences was 16 echoes in all cases, while the SE imaging was performed using a four echo, multiecho sequence.

RESULTS AND DISCUSSION

A pulse sequence diagram for the FSE sequence with an ETL of eight echoes is schematically shown in Fig. 1. An important feature to note about the sequence is that the phase is rewound after each echo to ensure that no residual phase is added onto the phase encode gradient applied to the later echoes of the same echo train. This rewinding also ensures that any stimulated echoes that may form at a later TE will have the correct phase for that echo. Figure 2 demonstrates the relationship

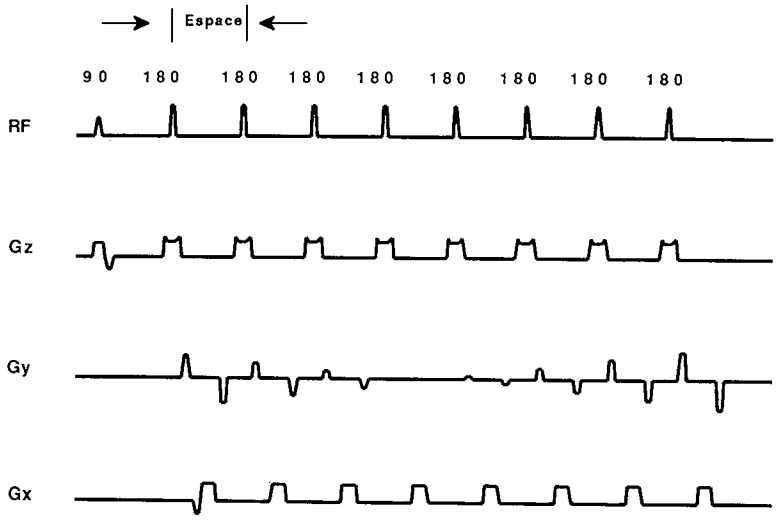

FIG. 1. Pulse sequence diagram for the FSE technique shown for an echo train length of eight echoes. The effective TE is determined by the E_{space} (time between consecutive echoes) and the echo number of the zeroth phase encode step. In this diagram the zeroth phase encode step occurs on the fourth echo, yielding an effective TE of $4*E_{space}$. Note also that the phase encode gradient (G_y) is rewound after each echo.

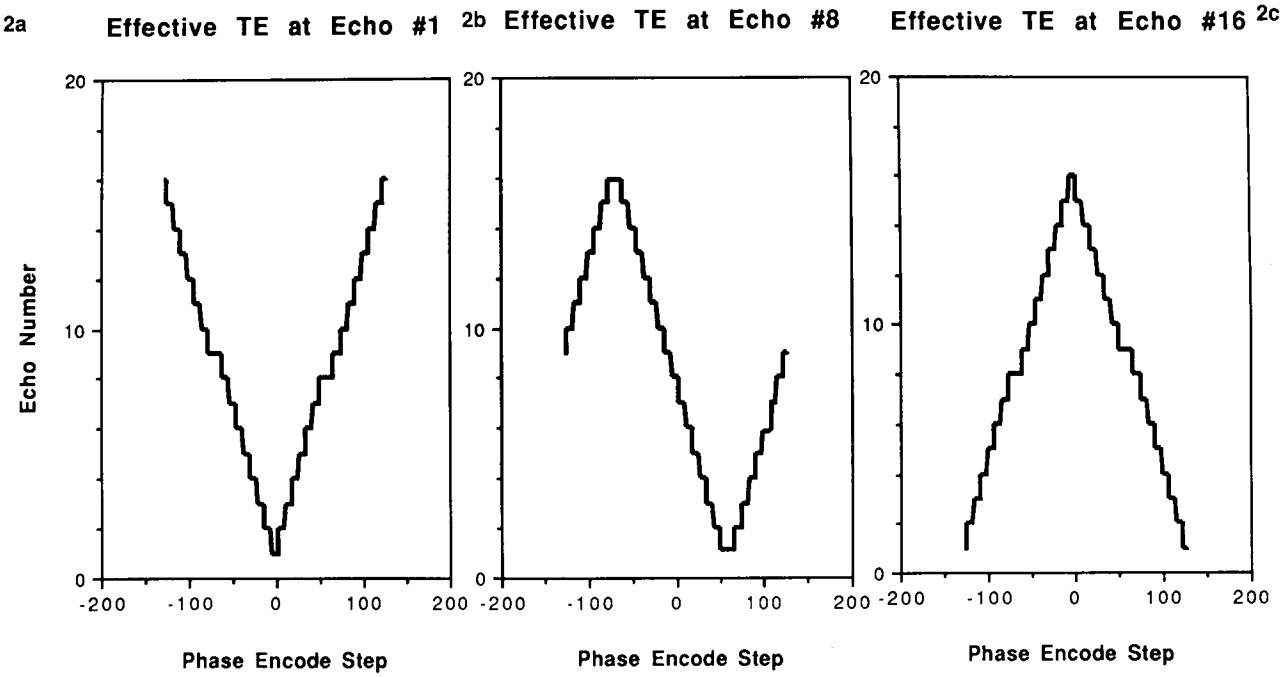

FIG. 2. Echo number versus phase encode step for three different effective TEs with an echo train length of 16 and an echo spacing of 20 ms between each echo in the echo train. The effective TE is determined by the echo number at which the zero and other low-order phase encode steps occur. **a:** The low-order phase encode gradients are placed on the first echo in the echo train, yielding an effective TE of 20 ms. **b:** The low-order phase encode steps are placed at the eighth echo, giving an effective TE of 160 ms. **c:** The low-order steps are placed at the last echo in the echo train, giving an effective TE of 320 ms.

between the phase encode order and the echo number in an echo train for three different effective TEs. The effective TE in this sequence is defined as that TE at which the lowest-order phase encodes are collected. The relationship between phase encode step and echo number is chosen in such a way as to produce the smoothest and narrowest PSF possible, while still covering all of phase encode steps and making full use of all 16 echoes in each echo train. If different phase encode lines are collected at different TEs, the T2 weighting of the lines will vary across the data set. It is this variable T2 weighting that leads to the PSF found in FSE imaging. A shorter ETL will result in a flatter signal response across the phase encode direction due to reduced T2 decay and hence a narrower PSF in the final image, although this will also increase imaging time. The PSF for a given tissue may be obtained by substituting the expression for TE(k), where k is the phase encode step, plotted in Fig. 2, into the signal strength equation for SE imaging. The Fourier transform of the resulting expression yields the PSF for that tissue under the selected imaging parameters. Figure 2 demonstrates that using an echo train of 16 echoes per 90° excitation pulse and an echo spacing of 20 ms within the echo train will lead to an effective TE of 20 ms if the low-order phase encodes are collected on the first echo (a), 160 ms if they are collected on the eighth echo (b), and 320 ms if the low-order phase encodes are collected on the last echo (c). Clearly, the effective PSF will be markedly different for the different effective TEs, and this can have important consequences on image quality (21).

Figure 3a and b demonstrates the SNR behavior of the FASE sequence and an SE sequence as a function of TE for three different tissues: gray and white matter and CSF. The figure demonstrates that the SNR per unit time and hence the efficiency of the pulse sequence is at least a factor of 8 higher in the FSE sequence than in the SE sequence. While the TR for the FSE sequence was higher (TR = 2,000 ms for SE vs. TR = 3,200 ms in FSE), this would contribute only an extra 5% signal in the FSE sequence, and so it is not the dominant factor in the SNR differences. (The length of time a conventional SE sequence would take using the same TR, ~28 min, precluded a comparison at this TR.) The changes in SNR as a function of TE for the different tissues are qualitatively similar for each pulse sequence, indicating that, as expected, the contrast behavior of the FSE sequence with changes in the effective TE is similar to that of a conventional SE sequence. The SNR of the FSE sequence is a function of the effective TE used, the ETL, and the spacing between consecutive echoes in an echo train, since these all affect the PSF of the imaging sequence. Since the PSF acts only to modulate the noise-free signal from different tissues and does not affect the noise level, the SNR will not be

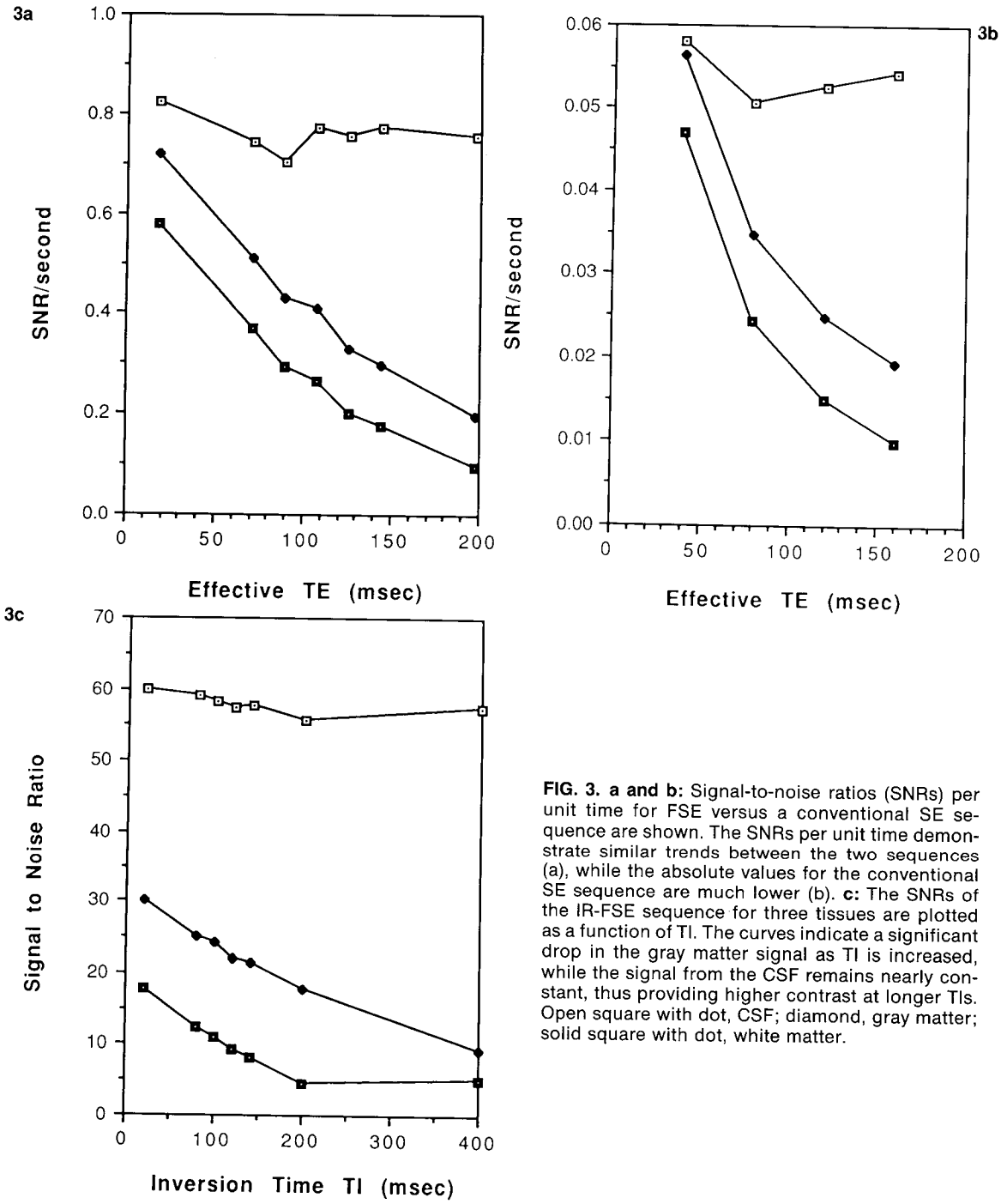

FIG. 3. a and b: Signal-to-noise ratios (SNRs) per unit time for FSE versus a conventional SE sequence are shown. The SNRs per unit time demonstrate similar trends between the two sequences (a), while the absolute values for the conventional SE sequence are much lower (b). **c:** The SNRs of the IR-FSE sequence for three tissues are plotted as a function of TI. The curves indicate a significant drop in the gray matter signal as TI is increased, while the signal from the CSF remains nearly constant, thus providing higher contrast at longer TIs. Open square with dot, CSF; diamond, gray matter; solid square with dot, white matter.

the same at all spatial frequencies or for all tissues. The CNRs per unit time for both the FSE and the SE sequences are given in Table 1 for two different effective TEs. The table clearly shows that the FSE sequence is by far the more efficient sequence and that very high contrast can be achieved in very short imaging times with this sequence.

Figure 3c demonstrates the SNR behavior of the IR-FSE sequence as a function of the TI. It also

TABLE 1. *Contrast-to-noise ratios per unit time for FSE versus conventional SE imaging*

	Gray/white matter		CSF/gray matter	
	FSE	SE	FSE	SE
TE = 80 ms	0.172	0.010	0.159	0.016
TE = 160 ms	0.126	0.009	0.362	0.035

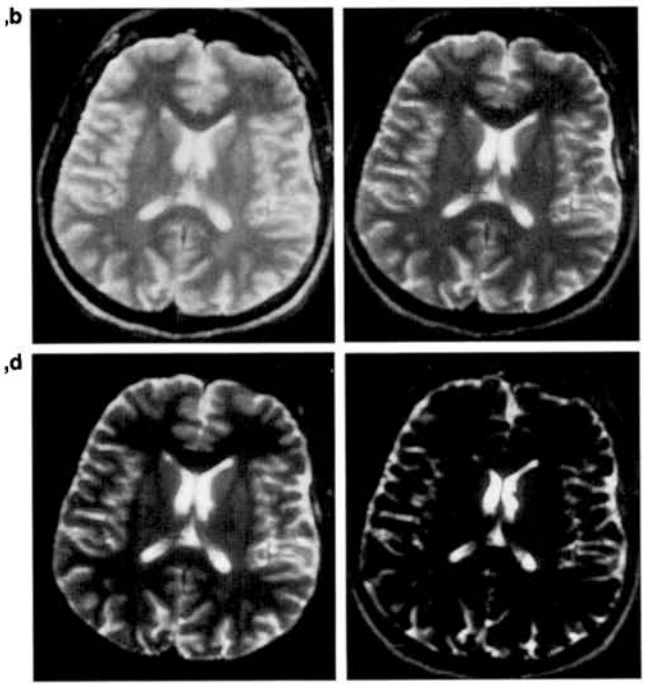

FIG. 4. FSE and IR-FSE images of a normal brain, 108/3,200 with no inversion pulse **(a)**, and inversion pulse added with TI = 20 ms **(b)**, TI = 100 ms **(c)**, and TI = 400 ms **(d)**.

demonstrates the high contrast that may be obtained between CSF and gray and white matter as TI is increased. For maximum contrast between gray and white matter and CSF, imaging should be performed at the null point of the fat, thereby allowing all of the gray scale contrast to be divided between the CSF and gray and white matter. Images demonstrating the increased contrast at TI = 100 ms are shown in the following figures.

The effect of applying the inversion pulse in IR-FSE is shown in Fig. 4. The imaging parameters are 3,200/108/1:50 with three different TIs: without an inversion pulse (a) and with an inversion pulse at TI = 20 ms (b), TI = 100 ms (c), and TI = 400 ms (d). The fat signal is suppressed for TI = 100 ms, although not completely. It has been our experience with clinical applications that incomplete nulling of the fat signal is advantageous as anatomic reference points are preserved. A TI of 143 ms was found to completely null the fat signal in body imaging. Contrast similar to that of regular STIR imaging (20) is obtained at TIs of $\geqslant$100 ms.

Figures 5 and 6 demonstrate current, high resolution, state-of-the-art fast MR imaging combining the FSE sequence with a phased array multicoil receiver (22,23). In Fig. 5, the top row shows consecutive sagittal images of the uterus obtained with the FSE sequence (4,500/126/4:49) and a phase array multicoil with a 20 cm field of view and a 512 × 256 matrix. Even with an anterior, in field of view saturation (SAT) pulse, there are motion artifacts from the high signal intraperitoneal fat. The bottom images are at similar locations in the same patient obtained using the IR-FSE sequence (TI = 100 ms) and a multiple coil array. The suppression of the fat signal in the IR-FSE sequence, even without SAT pulses, eliminates the motion artifact from the subcutaneous as well as the intraperitoneal fat.

In Fig. 6 high resolution FSE (a and b) and IR-FSE (c and d) sagittal images of the uterus are shown. The images were obtained using a phased array multicoil with a 20 cm field of view, 512 × 256 matrix, 4,500/126/4:49, and TI = 100 ms for the IR-FSE images. Figure 6 also shows high resolution FSE (e and f) and IR-FSE axial images (g and h) from the same patient as the sagittal images and obtained using the same imaging parameters. The images demonstrate very high resolution and excellent contrast and visibility of anatomical detail, particularly in distinguishing the zonal anatomy of the uterus, and show only minor motion artifact. The IR-FSE images appear to be superior in diagnostic quality, although clinical trials to test whether there is a diagnostic advantage to this technique over the FSE sequence have yet to be completed.

CONCLUSIONS

This article presents a demonstration of the SNR and CNR behavior of both FSE and IR-FSE imaging and compares this behavior to conventional SE imaging. The FSE sequences demonstrate superior image contrast and quality to the conventional SE technique and achieve this with much reduced imaging times. The addition of an inversion pulse to the FSE sequence either adds a slight additional time to the TR, and hence overall imaging time, or it may be absorbed through the loss of a slice or more, dependent upon the TI. When a short TI is used, images with contrast similar to conventional IR sequences are produced. In addition, when used with a multicoil array for high resolution pelvic imaging, the inversion pulse eliminates respiratory motion artifact from the anterior abdominal wall.

A drawback to the IR-FSE sequence and FSE itself is the high peak RF power deposition that ensues from the large number of 180° refocusing pulses (and the slice selective inversion pulses, one per echo train per slice, in IR-FSE). Calculations have indicated that the peak specific absorption rate in these sequences is still well below the federal guidelines. The advantages of using a SE fast imaging sequence include reduced susceptibility artifacts, field inhomogeneity, and chemical shift effects and the ability to move to long effective TEs, thereby producing heavily T2-weighted images with very short acquisition times.

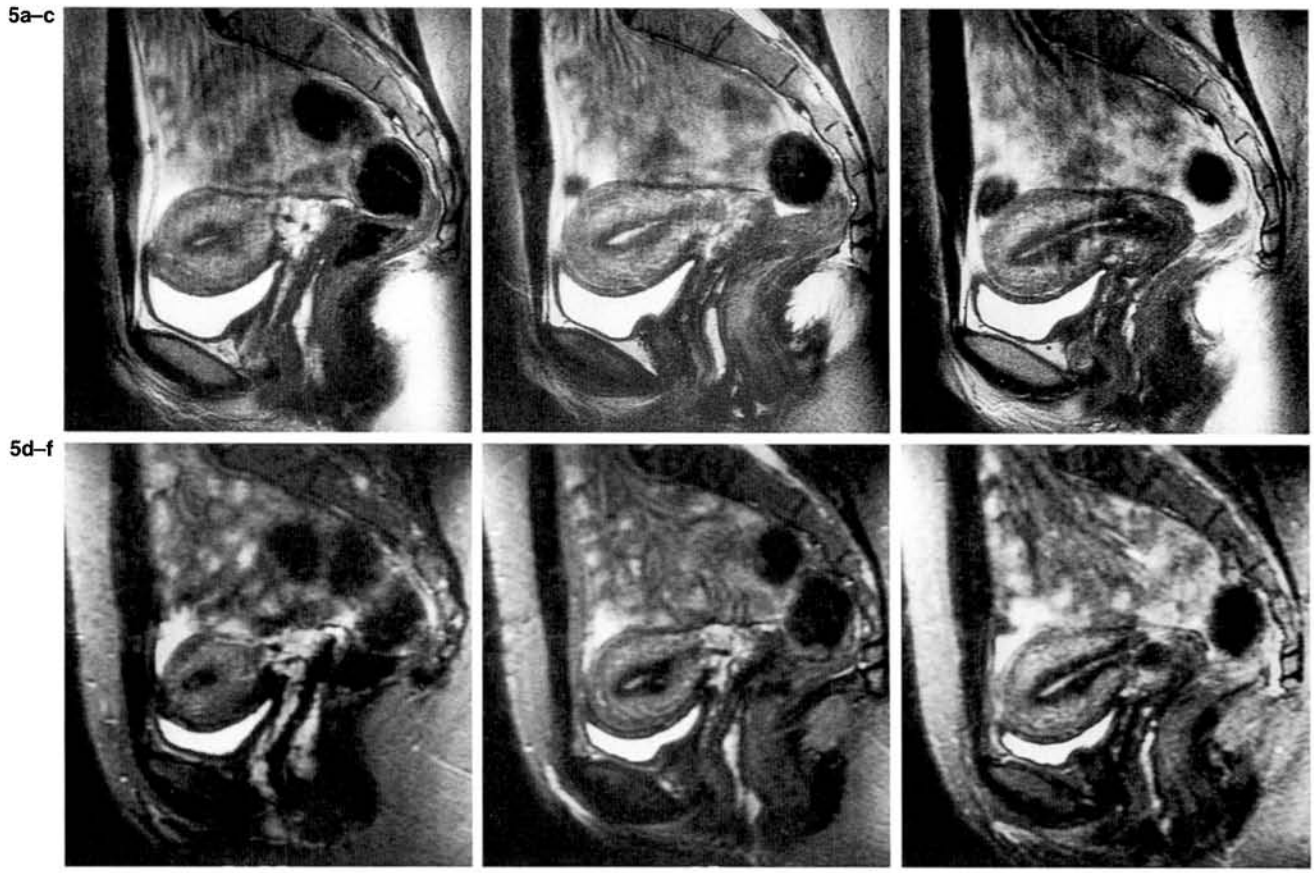

FIG. 5. Consecutive sagittal images of the uterus obtained with the FSE sequence (4,500/126) using a multicoil array with a 20 cm field of view and 512 × 256 matrix are shown **(a–c)**. Even with an anterior, in field of view saturation pulse, there remains motion artifact from the high signal intraperitoneal fat. The bottom row of images **(d–f)** are at similar locations in the same patient but were obtained using the IR-FSE sequence (TI = 100 ms) and a multicoil array. The suppression of the fat signal, even without the SAT pulses used in (a–c), eliminates the motion artifact from the subcutaneous as well as the intraperitoneal fat.

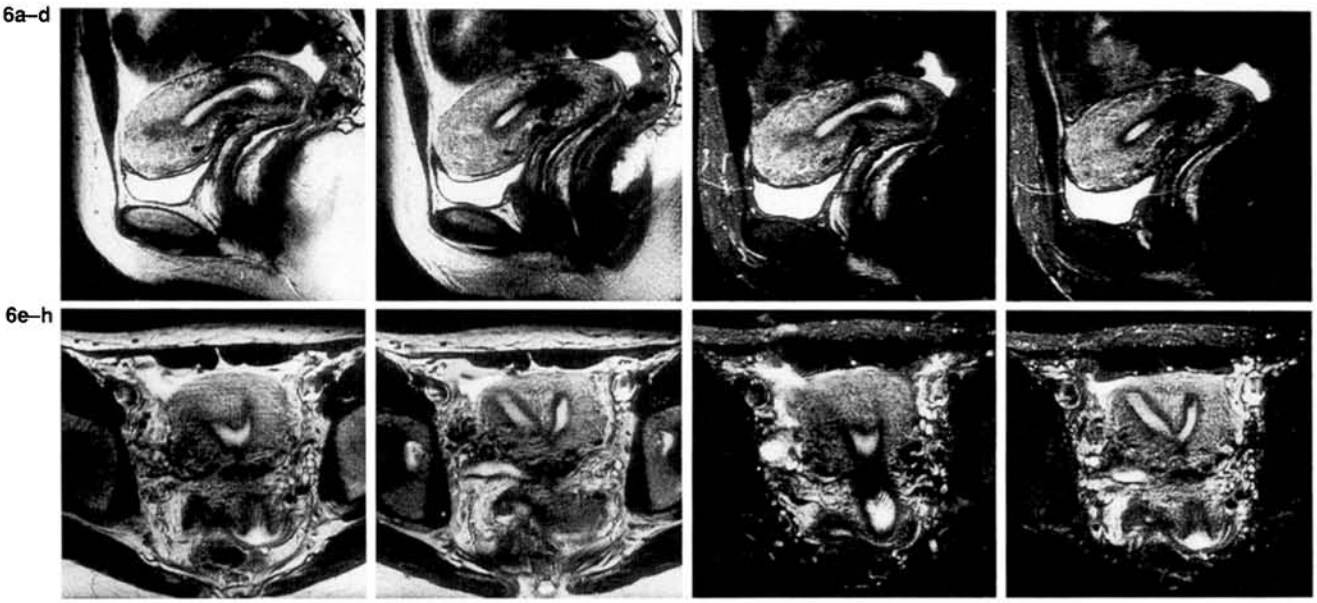

FIG. 6. High resolution multicoil FSE **(a,b)** and IR-FSE **(c,d)** sagittal images of the uterus obtained using a 512 × 256 matrix, 20 cm field of view, 4 mm slice thickness, and TR/TE of 4,500/126. Also shown are high resolution FSE **(e,f)** and IR-FSE **(g,h)** axial images of the same patient (TI = 100 ms in all IR-FSE images). The inversion pulse decreases the bright signal from subcutaneous fat and thus allows for increased contrast between the remaining soft tissues. The zonal anatomy of the uterus is well differentiated in all of the images, with the axial images clearly demonstrating the septate uterus.

Acknowledgment: The financial and technical support of General Electric Co. (Waukesha, WI) is gratefully acknowledged.

REFERENCES

1. Tkach JA, Haacke EM. A comparison of fast spin echo and gradient field echo sequences. *Magn Res Imag* 1988;6:373–89.
2. Van Der Meulen P, Groen JP, Tinus AMC, Bruntink G. Fast field echo imaging: an overview and contrast calculations. *Magn Res Imag* 1988;6:335–68.
3. Mansfield P. Real-time echo-planar imaging by NMR. *Br Med Bull* 1984;40:187–90.
4. Haase A, Frahm J, Matthaei D, Hanicke W, Merboldt K-D. FLASH imaging. Rapid NMR imaging using low flip-angle pulses. *J Magn Res* 1986;67:258–66.
5. Oppelt A, Graumann R, Barfub H, Fischer H, Hartl W, Schajor W. FISP—a new fast MRI sequence. *Electromedica* 1986;54:15.
6. Matthaei D, Haase A, Henrich D, Duhmke E. Cardiac and vascular imaging with an MR snapshot technique. *Radiology* 1990;177:527–32.
7. Winkler ML, Ortendahl DA, Mills TC, et al. Characteristics and partial flip angle and gradient reversal MR imaging. *Radiology* 1988;166:17–26.
8. Haacke EM, Tkach JA. Fast MR imaging: techniques and clinical applications. *AJR* 1990;155:951–64.
9. Holsinger AE, Riederer SJ. The importance of phase-encoding order in ultra-short TR snapshot MR imaging. *Magn Res Med* 1990;16:481–8.
10. Chien D, Atkinson DJ, Edelman RR. Strategies to improve contrast in turboFLASH imaging: reordered phase encoding and K-space segmentation. *J Magn Res Imag* 1991;1:63–70.
11. Hennig J, Nauerth A, Friedburg H. RARE imaging: a fast imaging method for clinical MR. *Magn Res Med* 1986;3:823–33.
12. Hennig J. Multiecho imaging sequences with low refocusing flip angles. *J Magn Res* 1988;78:397–407.
13. Van Uijen CMJ, Den Boef JH, Verschuren FJJ. Fast Fourier imaging. *Magn Res Med* 1985;2:203–17.
14. Haacke EM, Bearden FH, Clayton JR, Linga NR. Reduction of MR imaging time by the hybrid fast-scan technique. *Radiology* 1986;158:521–9.
15. Majumdar S, Orphanoudakis SC, Gmitro A, O'Donnell M, Gore JC. Errors in the measurements of T2 using multiple-echo MRI techniques. I. Effects of radio frequency pulse imperfections. *Magn Res Med* 1986;3:397–417.
16. Crawley AP, Henkelman RM. Errors in T2 estimation using multislice multiple echo imaging. *Magn Res Med* 1987;4:34–47.
17. Mulkern RV, Wong STS, Winalski C, Jolesz FA. Contrast manipulation and artifact assessment of 2D and 3D RARE sequences. *Magn Res Imag* 1990;8:557–66.
18. Higuchi N, Oshio K, Imai Y, et al. Clinical applications of multishot RARE in abdominal MR imaging. Proceedings of the SMRI 1991, abstr. 102, 1991.
19. Melki PS, Mulkern RV, Panych LP, Jolesz FA. Comparing the FAISE method with conventional dual-echo sequences. *J Magn Res Imag* 1991;1:319–26.
20. Bydder GM, Steiner GM, Blumgart LH, Khenia S, Young IR. MR imaging of the liver using short TI inversion recovery sequences. *J Comput Assist Tomogr* 1985;9:1084–9.
21. Constable RT, Gore JC. The loss of small object contrast in FASE imaging. Proceedings of the SMRM, Abstr. 1238, 1991.
22. Hayes CE, Roemer PB. Noise correlations in data simultaneously acquired from multiple surface coil arrays. *Magn Res Med* 1990;16:181–91.
23. Roemer PB, Edelstein WA, Hayes CE, Souza SP, Mueller OM. The NMR phased array. *Magn Res Med* 1990;16:192–225.